Title

Synthesis of nanocrystalline aluminum matrix composites reinforced with in situ devitrified Al-Ni-La amorphous particles

Journal

Scripta Materialia, 54(5)

ISSN

1359-6462

Authors

Zhang, Zhihui H
Han, B Q
Witkin, D
et al.

Publication Date

2006-03-01

Peer reviewed

Available online at www.sciencedirect.com
SCIENCE DIRECT
Scripta Materialia xxx (2006) xxx–xxx
Scripta MATERIALIA
www.actamat-journals.com

Synthesis of nanocrystalline aluminum matrix composites reinforced with in situ devitrified Al–Ni–La amorphous particles

Zhihui Zhang [a,*], Bing Q. Han [a], David Witkin [b], Leonardo Ajdelsztajn [a], Enrique J. Lavernia [a]

[a] Department of Chemical Engineering and Materials Science, University of California, Davis, CA 95616, USA
[b] Department of Chemical Engineering and Materials Science, University of California, Irvine, CA 92697, USA

Received 5 October 2005; received in revised form 31 October 2005; accepted 2 November 2005

Abstract

Nanocrystalline aluminum matrix composites were synthesized via hot extrusion of cryomilled 5083 Al (Al–4.59Mg–0.57Mn–0.25Fe in wt.%) blended with amorphous $Al_{85}Ni_{10}La_5$ powder. The compression yield strength of the as-extruded composite is 813 and 906 MPa for 10 and 20 vol.% $Al_{85}Ni_{10}La_5$, respectively. The observed thermal stability is discussed in light of the mechanical behavior.

Keywords: Metal matrix composites; Nanocrystalline; Amorphous; Nanoindentation; Al alloys

1. Introduction

Al-based, particulate reinforced metal matrix composites (MMCs) are of interest for structural applications, in part because their mechanical properties are isotropic and in some cases superior to those of conventional aluminum alloys [1,2]. Among the various MMCs that are currently being studied, ceramic particles such as silicon carbide (SiC) or alumina (Al_2O_3) are widely used as the reinforcement particles due to their advantages in terms of low density and high elastic modulus. However, interfacial decohesion or undesirable reactions represent major drawbacks that are frequently associated with ceramic particles reinforced MMCs [1,2]. Intermetallic compounds are an interesting reinforcement option in view of their low density and adequate elastic modulus in comparison with Al [3]. More importantly, stable chemical bonds could form at the interface between the reinforcement particles and the Al matrix. In many cases, however, chemical reactions or diffusion reactions at the interface remain as a major obstacle during materials processing and service at elevated temperatures. There are some aluminide intermetallic systems that are of interest due to the thermodynamic equilibrium state that can be established between the reinforcement and matrix. These include Al–Al_3Ni, Al–Al_3Ti, Al–Al_3Zr and Al–Al_3Fe systems [3]. The discovery of amorphous Al–TM–RE (TM = transition metals, RE = rare earth metals) alloys [4] provides a new family of reinforcement phases with the following potential attributes: (i) thermodynamically stable intermetallic phases could be formed via in situ devitrification reactions during powder metallurgy (P/M) processing; (ii) a nanocrystalline microstructure could be achieved due to their high nucleation density and low growth rate, thus providing a high fracture strength (>1000 MPa) [5]; (iii) the Al phase formed in the reinforcement particles could provide a compatible bond between the reinforcement particles and the Al matrix.

The present study was undertaken in an effort to explore the possibility of using a glass-forming $Al_{85}Ni_{10}La_5$ alloy [4] as a new type of reinforcement in nanostructured 5083 Al alloy produced via cryomilling. The

* Corresponding author. Tel.: +1 530 752 9568; fax: +1 530 752 1031.
E-mail address: zhizhang@ucdavis.edu (Z. Zhang).

1359-6462/$ - see front matter
doi:10.1016/j.scriptamat.2005.11.003

selection of 5083 Al/$Al_{85}Ni_{10}La_5$ nanocomposite was motivated by the following considerations: (i) formation of thermodynamic equilibrium phases (i.e., Al, Al_3Ni and $Al_{11}La_3$) in the $Al_{85}Ni_{10}La_5$ particles following complete devitrification [6]; (ii) retention of nanocrystalline microstructure in the $Al_{85}Ni_{10}La_5$ particles following a conventional P/M process route (e.g., degassing, cold isostatic pressing and extrusion); (iii) recent interest in Al-based alloys (composites) with ultrahigh strength (>1000 MPa).

2. Experimental procedure

The $Al_{85}Ni_{10}La_5$ powder was produced via atomization of a mixture of pure elemental Al (99.99%), Ni (99.9%) and La (99.9%) using helium gas (see Ref. [6] for details). Powder in the size range <25 μm was identified to be fully amorphous using X-ray diffraction (XRD) and was mechanically separated for use as a reinforcement. Two different volume fractions of reinforcement were selected: 10% and 20%. Prior to blending with the <25 μm $Al_{85}Ni_{10}La_5$ powder, the 5083 Al powder (with ~0.2 wt.% stearic acid) was cryomilled at approximately –190 °C for 8 h at a ball-to-powder ratio of 32:1 to achieve a nanocrystalline microstructure. Details of this process can be found in Refs. [7,8]. Prior to degassing, cold isostatic pressing was performed on the blends at 310 MPa for 5 min to obtain a green compact. Degassing was carried out at 400 °C until a vacuum of 10^{-6} Torr was attained (i.e., ~8 h). Following degassing the green compacts were extruded at 525 °C using a reduction ratio of 6.5:1. Some of the extrusions were further swaged at a temperature of 450 °C. The extrusion bar, with a diameter of ~19.3 mm, was swaged in four passes to a diameter of ~16.5 mm.

The microstructures of the composites were examined using XRD and transmission electron microscopy (TEM). The TEM was carried out using a Philips CM-12 electron microscope operating at 100 kV equipped with an energy dispersive X-ray spectrometer (EDX). The TEM specimens were prepared by twin-jet electropolishing in a solution of 33% nitric and 67% methanol at −35 °C.

The mechanical performance of the composites was characterized using nanoindentation and compression testing. The nanoindentation tests were performed in an MTS Nanoindenter XP using a standard Berkovich indenter. The compression tests were carried out at a strain rate of 10^{-3} in a universal testing machine (INSTRON 8801) using cylindrical specimens machined along the longitudinal direction to have both height and diameter equal to 4 mm. The displacement of compression platens (including the displacement of specimens and the elastic deformation of platens) was measured by a dual-camera video extensometer. The component of the elastic deformation of platens was subtracted from the compression stress–strain curves by measuring the elastic deformation of the compression platens without a specimen.

3. Results and discussion

3.1. Microstructure

Metallographic analysis of the composites indicates that the $Al_{85}Ni_{10}La_5$ particles are uniformly distributed in the 5083 Al matrix after consolidation. The amorphous $Al_{85}Ni_{10}La_5$ particles undergo complete crystallization (i.e., >~310 °C) during the P/M processing. As shown in the XRD pattern in Fig. 1, the crystallization products are identified as Al, Al_3Ni and $Al_{11}La_3$, confirming that they are in the thermodynamic equilibrium state corresponding to the Al–Ni–La phase diagram [9].

TEM results of the as-extruded microstructure (10% $Al_{85}Ni_{10}La_5$) are presented in Fig. 2, along with the corresponding selected area electron diffraction (SAED) patterns (inset). The grain size of the cryomilled 5083 Al matrix is approximately 200 nm (Fig. 2(a)); this is in agreement with results obtained for a 5083 Al alloy (i.e., average grain size ~207 nm) processed under similar processing conditions [8], indicating that the presence of $Al_{85}Ni_{10}La_5$ particles did not significantly influence the microstructural evolution of the 5083 Al matrix during the extrusion process. Compared with the matrix, the resultant grain size of the $Al_{85}Ni_{10}La_5$ particles is smaller (i.e., <200 nm), as shown in Fig. 2(b), suggesting that the nanocrystalline $Al_{85}Ni_{10}La_5$ (nc-$Al_{85}Ni_{10}La_5$) particles have intrinsically better thermal stability. The thermal stability of this composite will be further discussed in a subsequent section. The corresponding SAED pattern (inset) shows a typical ring pattern resulting from nanocrystalline grains that are separated by large angle grain boundaries, implying that the nanocrystalline Al, Al_3Ni and $Al_{11}La_3$ phases were randomly separated from one another. As is shown later on, the homogeneous distribution of Al, Al_3Ni and $Al_{11}La_3$ phases was also evident from EDX analysis. Fig. 2(c) reveals a grain-boundary-like interface (as indicated by arrows) is formed between the $Al_{85}Ni_{10}La_5$ particles and the matrix. The formation of a metallurgical bond between the two components of the composite allows the

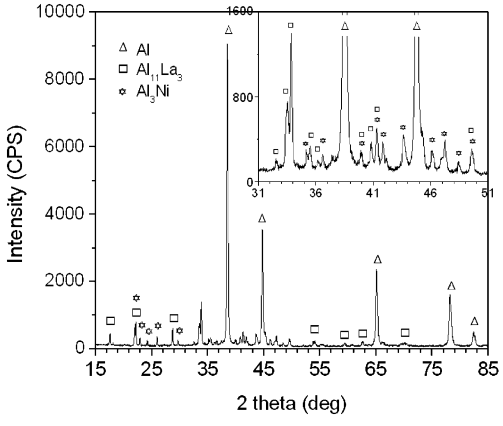

Fig. 1. XRD pattern of 5083 Al/$Al_{85}Ni_{10}La_5$ nanocomposite.

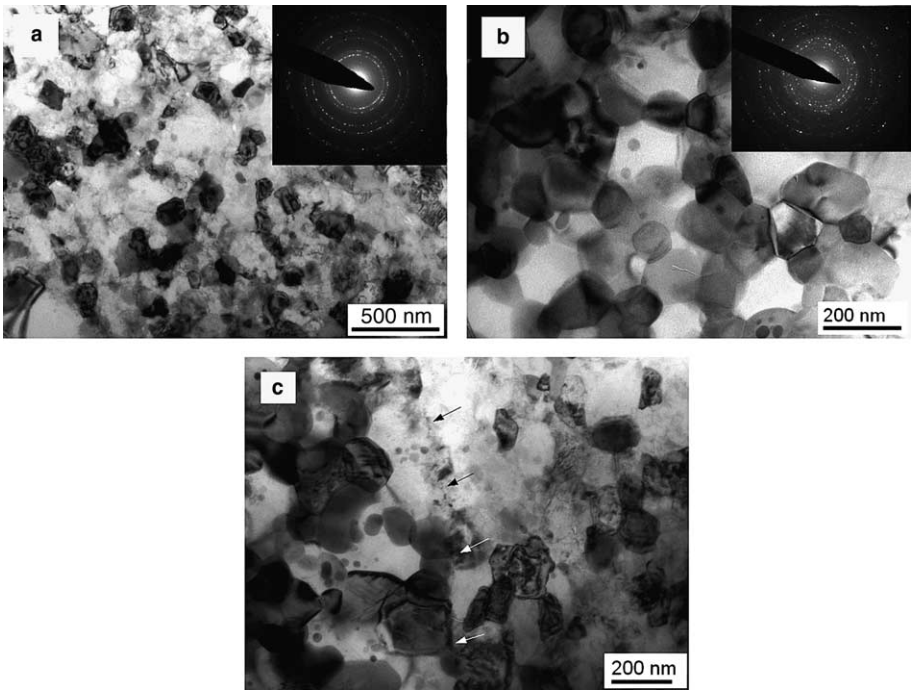

Fig. 2. TEM micrographs of as-extruded 5083 Al/$Al_{85}Ni_{10}La_5$ composite: (a) 5083 Al matrix, (b) $Al_{85}Ni_{10}La_5$ particles, and (c) the interface region indicated by arrows.

load to be effectively transferred from the matrix to the reinforcements.

3.2. Nanoindentation

In order to evaluate the reinforcing efficiency of the nc-$Al_{85}Ni_{10}La_5$ particles, nanoindentation was performed to measure their hardness and elastic modulus. The hardness is determined from the unloading curve using the method proposed by Oliver and Pharr [10] and the elastic modulus is determined from the loading curve by continuous stiffness measurements [11]. In order to minimize the indentation size effect [12,13], an indentation depth of 700 nm was used for the nc-$Al_{85}Ni_{10}La_5$ particles. The measurements for the intermetallic compounds $Al_{11}La_3$ and Al_3Ni were performed on coarse dendrites in an $Al_{85}Ni_{10}La_5$ cast ingot with a depth size of 500 nm. Table 1 summarizes the measured results along with the calculated theoretical densities. The nc-$Al_{85}Ni_{10}La_5$ has a hardness of approximately 3.93 GPa and a density of 3.53 g/cm^3. The elastic modulus of the nc-$Al_{85}Ni_{10}La_5$ is determined to be approximately 120 GPa, which is significantly higher than that of 5083 Al (i.e., 71 GPa [14]), indicating that the nc-$Al_{85}Ni_{10}La_5$ is a good reinforcement candidate for Al-based MMCs. For comparison purposes, the elastic modulus of the nanostructured 5083 Al in the present study is determined to be approximately 74 GPa and the deviation is less than 5%, suggesting the elastic moduli determined using the indentation techniques is quite reasonable.

Table 1
Elastic modulus, density and hardness of reinforcements

	Elastic modulus (GPa)	Calculated density (g/cm^3)	Hardness (GPa)
Al_3Ni[a]	200	3.98	11.33
$Al_{11}La_3$[a]	140	4.01	7.54
nc-$Al_{85}Ni_{10}La_5$[b]	120	3.53	3.93

[a] Measured with an indentation depth of 500 nm.
[b] Measured with an indentation depth of 700 nm.

3.3. Mechanical properties

Fig. 3(a) shows the compression true stress vs. true strain curves for the as-extruded composites with 10% and 20% nc-$Al_{85}Ni_{10}La_5$ particles and the as-swaged composite with 10% nc-$Al_{85}Ni_{10}La_5$ particles. For comparison purposes, a compression true stress vs. true strain curve for a 100% cryomilled 5083 Al alloy processed using the same processing route and a tensile true stress vs. true strain curve for a conventional 5083 Al alloy are also plotted in Fig. 3(a). The nc-$Al_{85}Ni_{10}La_5$ particles significantly increase the yield strength (0.2% offset) of cryomilled 5083 Al alloy. The addition of 10% nc-$Al_{85}Ni_{10}La_5$ particles increased the yield strength to 813 MPa from 681 MPa for the cryomilled 5083 Al alloy while the addition of 20% nc-$Al_{85}Ni_{10}La_5$ led to an increase to 906 MPa. Fig. 3(b) presents the yield strength as a function of reinforcement volume fractions. The yield strength increases linearly with increasing volume fraction (V_p) of nc-$Al_{85}Ni_{10}La_5$ particles, suggesting that the strengthening behavior follows a rule of mixtures ($\sigma = (1 - V_p)\cdot\sigma_m +$

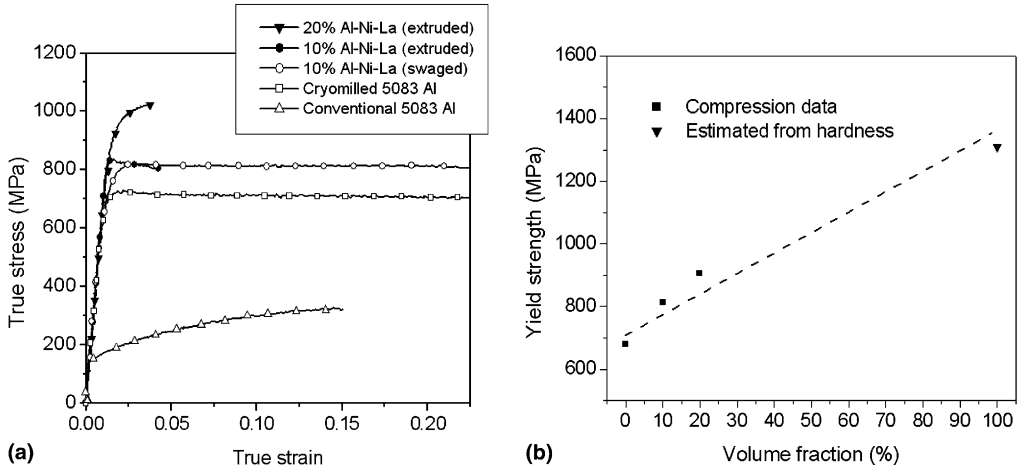

Fig. 3. (a) True stress–strain curves of 5083 Al/$Al_{85}Ni_{10}La_5$ composites. (b) Volume fraction dependence of yield strength for the as-extruded composites.

$V_p \cdot \sigma_p$, where σ_m and σ_p are the yield strength of matrix and particulates, respectively. σ_p is estimated from the hardness value, i.e., $\sigma_p \approx H/3$). A rule-of-mixtures behavior was also observed in bimodal nanostructured Al alloys in which coarse-grained particles were introduced to improve the ductility [7,8], although in that case the strength of bimodal Al alloys decreased with increasing volume fraction of soft coarse-grained regions.

The stress–strain curves of the 5083 Al/$Al_{85}Ni_{10}La_5$ composites exhibit elastic–nearly perfectly plastic behavior with a brief region of strain hardening. This characteristic is also observed in many other bulk nanocrystalline or ultrafine-grained materials [15–17] or bimodal materials [8]. The stress–strain behavior has been generally rationalized using a framework of dislocation-mediated plasticity. Hayes et al. [17] proposed that dislocation motion initiated within the larger grains at the yield point, and when the stress in the coarse-grained regions reached a threshold, deformation commenced in finer grained regions. In the present composites, the stress should further transfer to the nc-$Al_{85}Ni_{10}La_5$ particles, thereby yielding a higher flow stress.

The as-extruded composites exhibit a limited failure strain, which is approximately 3.3% for the 10% nc-$Al_{85}Ni_{10}La_5$ composite and 2.4% for the 20% nc-$Al_{85}Ni_{10}La_5$ composite, respectively. Inspection of the fracture surface using SEM reveals debonding between the nc-$Al_{85}Ni_{10}La_5$ particles and 5083 Al matrix (not shown here). In a cryomilled Al–10Ti–2Cu alloy, it was reported that fracture occurred primarily by nucleation and growth of voids at interfaces between the matrix and intermetallic particles [17]. The debonding between Al–Al grains observed in the present study may most likely be attributed to the impurity enrichment (e.g., oxide layers at the prior particle boundaries) at the interface; further work will be needed to address this issue, although the results obtained with the swaged material (see next section) support this hypothesis. In order to improve the ductility of the current material, two strategies may be considered. The first is to further increase the bonding strength at the reinforcement–matrix interface, i.e., to further break up any remaining oxide layers and eliminate residual porosity. Second, to promote plastic deformation such as introducing coarse grains, which has been suggested as an effective way for ductility improvement in nanostructured or ultrafine-grained material, either through introducing coarse-grained powder prior to consolidation [7,8] or through secondary processing (e.g., thermal annealing) [16,18,19].

In this study, swaging was used as a tool to investigate the influence of additional plasticity on ductility. Zhou et al. [20] studied the microstructural evolution of a nanostructured Al–Mg alloy during thermal annealing and suggested that subgrain rotation and coalescence play an important role in the formation of coarse grains in the nanostructured material. During a thermomechanical process such as swaging, grain coarsening and coalescence are accelerated during deformation as the orientation between adjacent grains changes in response to an applied load [21]. Recrystallization at heterogeneous sites [20] may also lead to the occurrence of coarse grains; this is observed in a nanostructured 5083 Al alloy under uniaxial compression at elevated temperatures [22]. In addition to the formation of coarse grains, the plasticity that is introduced during swaging will eliminate residual processing defects (e.g., porosity and prior particle boundaries) thereby increasing the bond strength between the reinforcement and matrix. As shown in Fig. 3(a), following swaging the 10% nc-$Al_{85}Ni_{10}La_5$ composite shows a significant improvement in the compressive ductility (i.e., a true strain of 22.5% without failure) while the compressive yield strength and flow stress is maintained. It is worth mentioning, however, that no significant grain growth occurred in the fine-grained region in the as-swaged 10% nc-$Al_{85}Ni_{10}La_5$ composite, as shown in Fig. 4. In terms of the coarse-grained regions, TEM observation reveals the grain size in the coarse region to be in the range of 600–2000 nm; this is in agreement with the results reported in other studies on cryomilled Al–Mg alloys, involving either the addition of

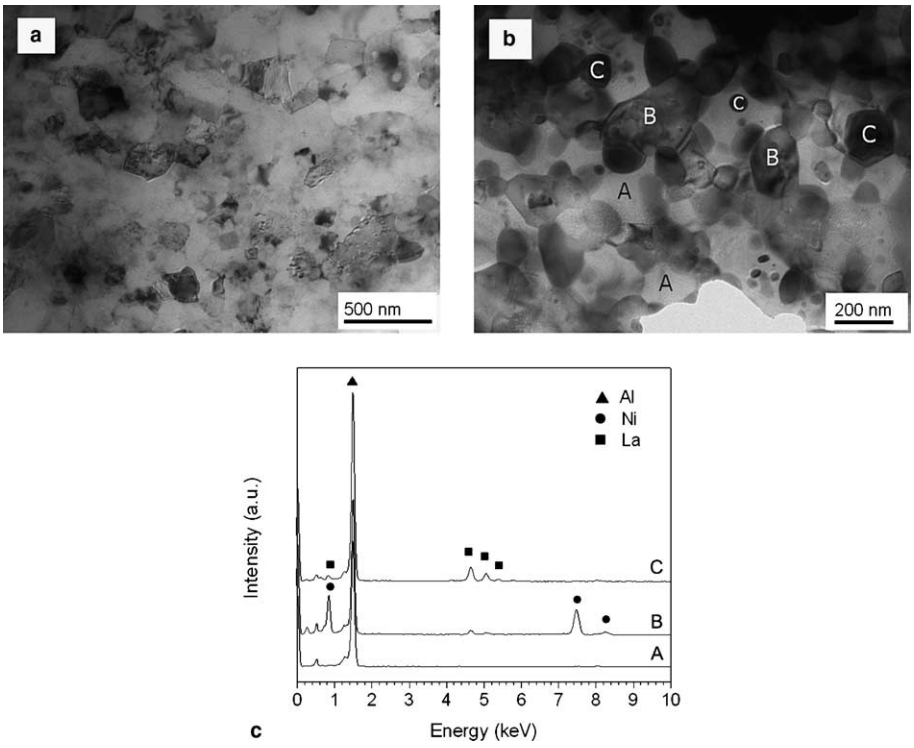

Fig. 4. TEM bright field images of as-swaged 5083 Al/$Al_{85}Ni_{10}La_5$ composite: (a) 5083 Al matrix, (b) $Al_{85}Ni_{10}La_5$ particles; (c) the EDX spectra of phase A, B and C that are marked in (b).

coarse-grained particles [7], thermal annealing [19], or uniaxial compression at elevated temperatures [22]. The presence of multiple scales in the microstructure leads to additional complexities in the evaluation of the volume fraction of coarse-grained regions via statistical counting of individual grains in TEM micrographs, since they are highly dependent on the transparent regions of individual specimens. However, as shown in Fig. 3(a), the longer strain hardening region in the as-swaged composite suggests that there is an increase in the volume fraction of coarse grains after swaging. The yield stress for the as-swaged sample decreases to 729 MPa from the initial value of 813 MPa in the as-extruded state.

3.4. Thermal stability

No significant grain growth was observed in 5083 Al/$Al_{85}Ni_{10}La_5$ composites after processing, despite the presence of thermal activation. A recent study of the creep behavior of the cryomilled 5083 Al alloy shows that its microstructure is extremely stable at elevated temperatures. After a long exposure at temperatures of 300 and 350 °C (i.e., >900 h), there is only limited grain growth [23]. Such unusual thermal stability has been generally rationalized by grain boundary segregation [24], grain boundary drag by solute elements [25], and second phase pinning [26], i.e., due to the formation of a small amount of nanoscale aluminum oxide, nitride and carbide dispersions during the cryomilling process resulting from the incorporation of N derived from the liquid nitrogen and other light elements (O, C, and H) from organic process control agents (e.g., stearic acid), stable oxide layers on Al particles, and contamination by atmospheric moisture [27].

The nc-$Al_{85}Ni_{10}La_5$ particles exhibit remarkable thermal stability during the P/M processing. The kinetic stabilization that is responsible for the sluggish growth in the nc-$Al_{85}Ni_{10}La_5$ particles is attributed to the unusually high nucleation density (>10^{21}) and the sluggish solute diffusivity which limits growth [28,29]. At elevated temperatures (>310 °C), the complete devitrification of amorphous $Al_{85}Ni_{10}La_5$ particles results in formation of equilibrium phase Al, Al_3Ni and $Al_{11}La_3$ in a eutectic-like transformation [6]. As shown in Fig. 4(b) and (c), the Al, Al_3Ni and $Al_{11}La_3$ phases that are identified by means of EDX are homogeneously distributed. Further growth of the crystallites requires consumption of their smaller identical species via long-range diffusion of Ni and La atoms. In comparison with Al and Ni, the rare earth metal La, however, has the lowest diffusivity in Al. As a result, the $Al_{11}La_3$ phase that results in smaller particle size should prevent the migration of Al and Al_3Ni phase boundaries. As shown in Fig. 4(b), the $Al_{11}La_3$ phase has the smallest grain size, confirming that the growth is primarily limited by the sluggish diffusivity.

4. Conclusions

Nanocrystalline 5083 Al/$Al_{85}Ni_{10}La_5$ composites are synthesized via a combination of cryomilling 5083 Al alloy and devitrification of amorphous $Al_{85}Ni_{10}La_5$ alloy. A P/M routine consisting of cold isostatic pressing, degassing,

extrusion and swaging is used to consolidate the powder blends. The $Al_{85}Ni10La_5$ particles are uniformly distributed in the 5083 Al matrix with the formation of good metallurgical bonds. The as-extruded nanocomposites exhibit ultrahigh compression strength and limited ductility but a good balance between the strength (e.g., yield strength of 729 MPa with 10% addition) and ductility (e.g., ~22.5%) is observed in the as-swaged composite. The high thermal stability is observed in both the nanocrystalline matrix and nanocrystalline reinforcement particles, suggesting that the composite is a promising candidate material for high temperature applications.

Acknowledgements

The authors would like to acknowledge the Army Research Office (Grant No. DAAD 19-03-1-0020) for financial support. Particular thanks also go to Dr. William Mullins for his support and assistance.

References

[1] Lloyd DJ. Int Mater Rev 1994;39:1.
[2] Srivatsan TS, Sudarshan TS, Lavernia EJ. Prog Mater Sci 1995;39:317.
[3] Varin RA. Metall Mater Trans A 2002;33:193.
[4] Inoue A. Prog Mater Sci 1998;43:365.
[5] Kawamura Y, Mano H, Inoue A. Scripta Mater 2001;44:1599.
[6] Zhang Z, Witkin D, Lavernia EJ. J Non-Cryst Solids 2005;351:1646.
[7] Witkin D, Lee Z, Rodriguez R, Nutt S, Lavernia EJ. Scripta Mater 2003;49:297.
[8] Han BQ, Lee Z, Witkin D, Nutt S, Lavernia EJ. Metall Mater Trans A 2005;36:957.
[9] Godecke T, Sun W, Luck R, Lu K. Z Metallkd 2001;92:717.
[10] Oliver WC, Pharr GM. J Mater Res 1992;7:1564.
[11] Li X, Bhushan B. Mater Charact 2002;48:11.
[12] Nix WD, Gao HJ. J Mech Phys Solids 1998;46:411.
[13] Feng G, Nix WD. Scripta Mater 2004;51:599.
[14] ASM handbook. Materials Park (OH): ASM International; 1990.
[15] Jia D, Ramesh KT, Ma E. Acta Mater 2003;51:3495.
[16] Han BQ, Lee Z, Nutt SR, Lavernia EJ, Mohamed FA. Metall Mater Trans A 2003;34:603.
[17] Hayes RW, Rodriguez R, Lavernia EJ. Acta Mater 2001;49:4055.
[18] Wang YM, Chen MW, Zhou FH, Ma E. Nature 2002;419:912.
[19] Han BQ, Mohamed FA, Bampton CC, Lavernia EJ. Metall Mater Trans A 2005;36:2081.
[20] Zhou F, Liao XZ, Zhu YT, Dallek S, Lavernia EJ. Acta Mater 2003;51:2777.
[21] Jin M, Minor AM, Stach EA, Morris JJW. Acta Mater 2004;52:5381.
[22] Witkin D, Han BQ, Lavernia EJ. J Mater Res 2005;20:2117.
[23] Han BQ, Zhang Z, Lavernia EJ. Philos Mag Lett 2005;85:97.
[24] Weissmuller J. Nanostruct Mater 1993;3:261.
[25] Michels A, Krill CE, Ehrhardt H, Birringer R, Wu DT. Acta Mater 1999;47:2143.
[26] Zhou F, Lee J, Lavernia EJ. Scripta Mater 2001;44:2013.
[27] Tellkamp VL, Melmed A, Lavernia EJ. Metall Mater Trans A 2001;32:2335.
[28] Allen DR, Foley JC, Perepezko JH. Acta Mater 1998;46:431.
[29] Hono K, Zhang Y, Inoue A, Sakurai T. Mater Trans JIM 1995;36:909.